Journal of Microscopy, Vol. 202, Pt 2, May 2001, pp. 446–450.
Received 28 August 2000; accepted 1 December 2000

Spectroscopic scanning near-field optical microscopy with a free electron laser: CH_2 bond imaging in diamond films

A. CRICENTI*, R. GENEROSI*, M. LUCE*, P. PERFETTI*, G. MARGARITONDO†, D. TALLEY‡, J. S. SANGHERA‡, I. D. AGGARWAL‡, J. M. GILLIGAN§ & N. H. TOLK§
*Istituto di Stuttura della Materia, via Fosso del Cavaliere 100, 00133 Roma, Italy
†Institut de physique appliquée, Ecole Polytecnique Fédérale, CH-1015 Lausanne, Switzerland
‡Optical Sciences Division, U.S. Naval Research Laboratory, 4555 Overlook Ave SE, Washington, DC 20375, U.S.A.
§Department of Physics and Astronomy, Vanderbilt University, Nashville, TN, U.S.A.

Key words. Diamond, free electron laser (FEL), scanning near-field optical microscopy (SNOM).

Summary

Hydrogen chemistry in thin films and biological systems is one of the most difficult experimental problems in today's science and technology. We successfully tested a novel solution, based on the spectroscopic version of scanning near-field optical microscopy (SNOM). The tunable infrared radiation of the Vanderbilt free electron laser enabled us to reveal clearly hydrogen-decorated grain boundaries on nominally hydrogen-free diamond films. The images were obtained by SNOM detection of reflected 3.5 μm photons, corresponding to the C–H stretch absorption, and reached a lateral resolution of 0.2 μm, well below the λ/2 (λ = wavelength) limit of classical microscopy.

Reflection scanning near-field optical microscopy (SNOM) conditions are reached when the light is collected by a narrow (< λ) fibre tip aperture, whose distance from the sample surface is also <λ; this breaks the aforementioned classical microscopy resolution limit, which is valid for far-field optics. SNOM imaging was achieved by many authors (Heinzelmann & Pohl, 1994; Betzig & Trautman, 1992; Pohl & Courjon, 1992; Betzig *et al.*, 1994; Almeida *et al.*, 1996; Cricenti *et al.*, 1998a) but the spectroscopic version of this technique is still quite rare, and it was never previously applied to H-related modes. This is a severe limitation, as microscopic-scale hydrogen detection is fundamentally important for a huge variety of problems in biology, polymer chemistry and materials science in general.

The biggest problems is the source: one needs an intense and tunable photon source to match the relevant absorption bands. Intensity is a critical point because of the inefficient light transmission of the narrow fibre tip. Free electron laser (FEL) sources are ideal solutions for this problem because of their unique combination of extreme intensity and broad tunability.

A detailed descriptions of the Vanderbilt FEL, active in the 1–10 μm spectral range, has already been given (Coluzza *et al.*, 1992; Tuncel *et al.*, 1993). SNOM images were obtained for the first time with an FEL using this source in 1998 (Cricenti *et al.*, 1998a). The corresponding multitechnique SNOM module has been described by Cricenti *et al.*, 1998b, see the schematic experimental set-up of Fig. 1; one should stress that this instrument can deliver shear-force (topographic) non-SNOM images as well as reflectivity, transmission and evanescent-wave SNOM images. The comparison of topographic and SNOM images is crucially important, and enables us to prove that no artefacts exist in the present SNOM images. Another crucial point was the fabrication of extremely high quality fibre tip points, as described by Mossadegh *et al.*, 1998.

Our tests were performed on artificial polycrystalline diamond films grown by plasma-assisted chemical vapour deposition (CVD) (Angus *et al.*, 1968). In principle, these should be hydrogen-free specimens after annealing to remove residual hydrogen and water. We

Correspondence to: A. Cricenti. Tel.: ; fax: ; e-mail:

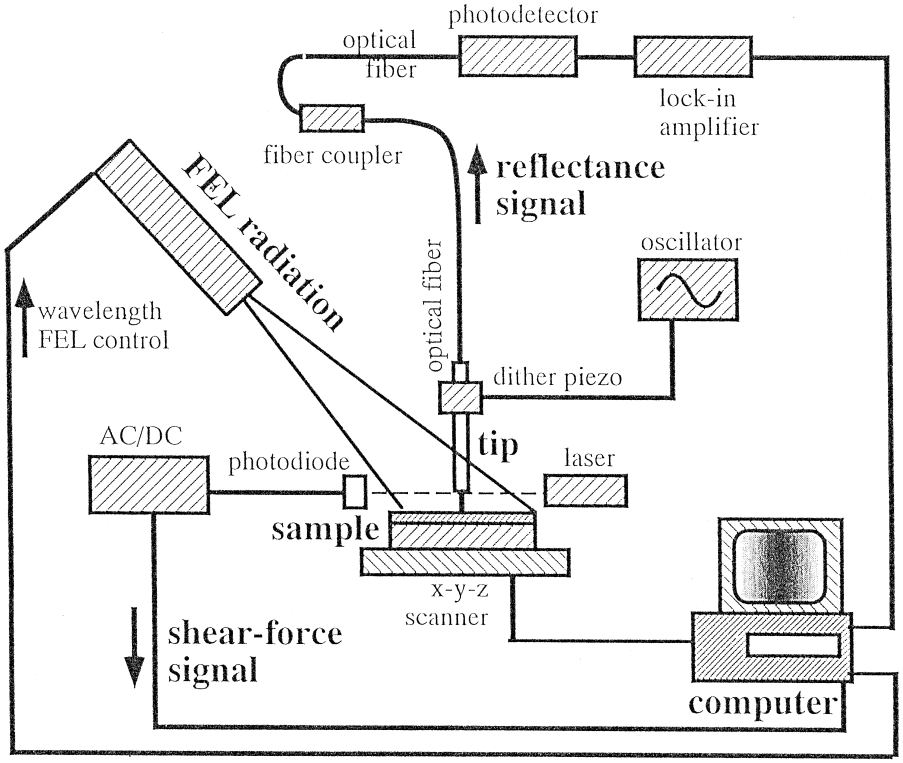

Fig. 1. Schematic diagram of our experimental set-up (see Cricenti *et al.*, 1998b). The FEL photons are sent to the sample surface and detected after reflection by a narrow-point optical fibre tip mounted on a SNOM module. The module can also deliver shear–force (topographic) images. The shear–force signal is independently used to keep the tip–surface distance constant while taking SNOM images. A lock-in amplifier is used to detect the modulated reflectivity signal, whereas the AC/DC converter is used to detect the shear–force amplitude. Optical fibre tip fabrication was a crucial issue. Infrared SNOM probes were obtained from single-mode arsenic sulphide fibres (with outer diameter of 80–140 μm and core diameter 10 μm), using a micropipette puller and heating by a filament or a laser (Mossadegh *et al.*, 1998).

tested precisely this point by tuning the FEL to $\lambda = 3.5$ μm, corresponding to a C-H vibrational stretch mode absorption band (see Fig. 2). The presence of such a band indicates that some hydrogen has been left on the sample after annealing.

Figure 3 (left-hand side) shows three 10×10 μm^2 SNOM reflection images obtained with $\lambda = 3.5$ μm photons (Fig. 3(c)) and with two adjacent wavelengths, $\lambda = 3.25$ μm (Fig. 3(a)) and $\lambda = 3.7$ μm (Fig. 3(e)), outside the absorption band of Fig. 2. In the reflection images darker areas correspond to stronger absorption. The contrast between the two featureless images off-absorption and the microstructure of the on-absorption image is striking. Moreover, the two off-absorption images give an indication on the value of the optical and electronic noise (around 0.01–0.02 mV, i.e. 10% of the signal measured at 3.5 μm).

The reflection Fig. 3(c) taken with 3.5 μm shows different reflection areas whose width ranges between 500 nm and 1500 nm, with signal variations of the

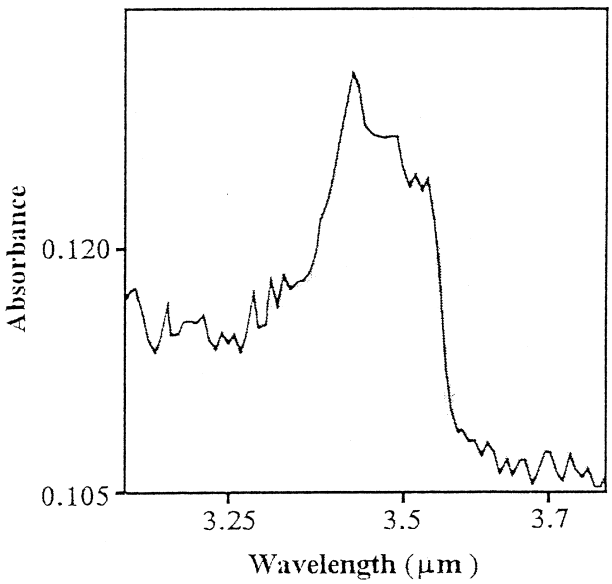

Fig. 2. Optical absorption spectrum, showing the $\lambda = 3.5$ μm, C–H vibrational stretch mode absorption band.

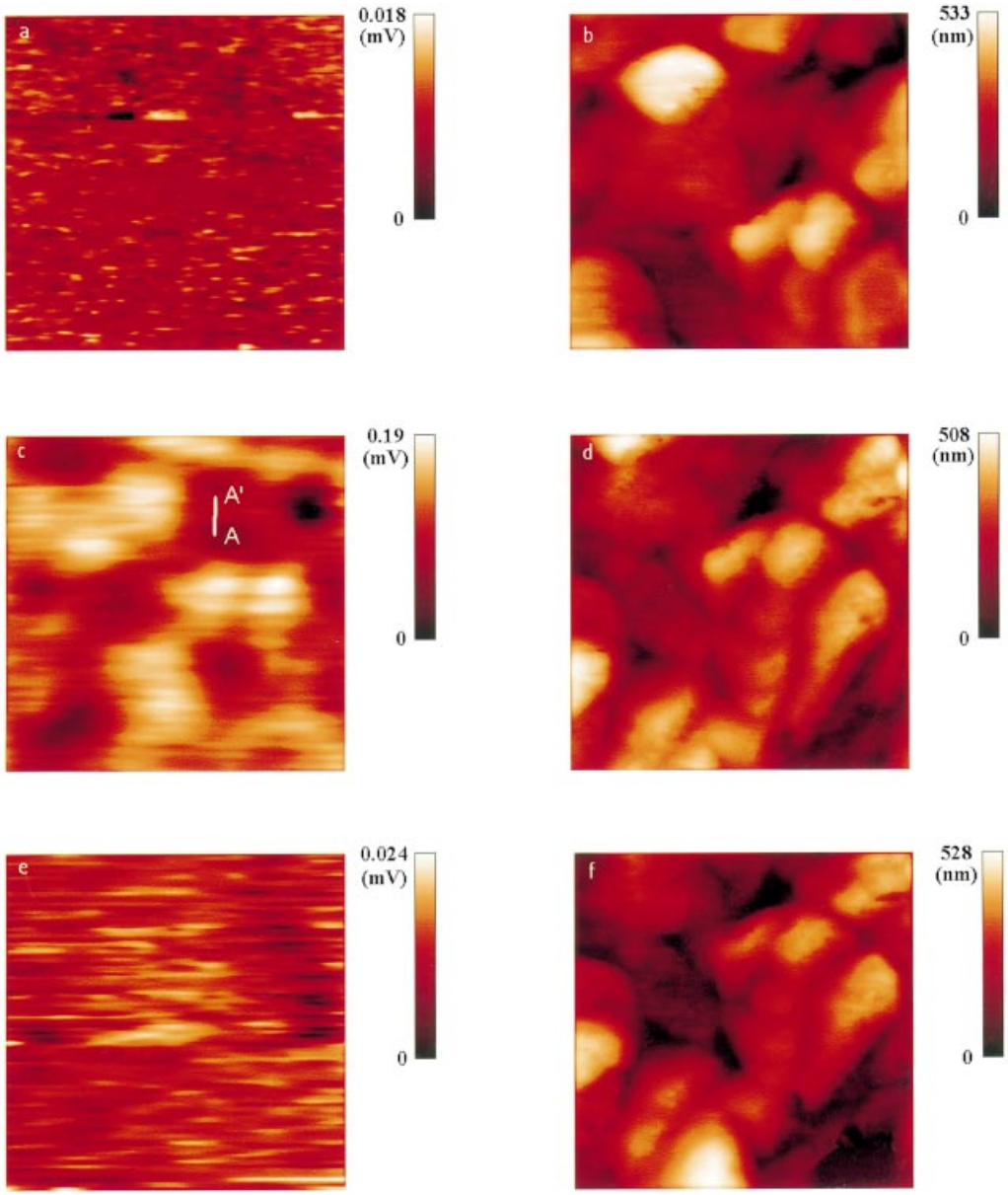

Fig. 3. Left: 10 × 10 μm^2 SNOM reflection images obtained with λ = 3.5 μm (C-H stretch absorption) photons (c) and with two adjacent wavelengths outside the absorption band: λ = 3.25 μm (a) and λ = 3.7 μm (e). Darker areas correspond to stronger absorption. Right: corresponding shear-force (topographic) images; brighter areas correspond to higher topography values. All the images shown are unfiltered and raw except for subtraction of a constant background.

order of 0.15–0.2 mV. Are this microstructures really related to hydrogen or are they just artefacts? The answer is provided by comparison with the corresponding shear–force (topological) image of Fig. 3(d). First of all, the same topological image is observed at the three different wavelengths, apart from a rigid shift of 1–2 μm in the *y* direction between Figs 3(b) and (d) and (f). Such a topological image shows the presence of diamond grains with a width of few micrometres and an height of few hundred nanometres. Absolutely no one-to-one correlation is observed between topological and SNOM image features, ruling out artefacts. This proves, in fact, that the dark regions in the on-absorption SNOM image of Fig. 3(c) correspond to regions with strong H-related absorption, i.e. where residual hydrogen is present in the film.

It is worth pointing out the possibility that topographical shadow effects might be present in SNOM

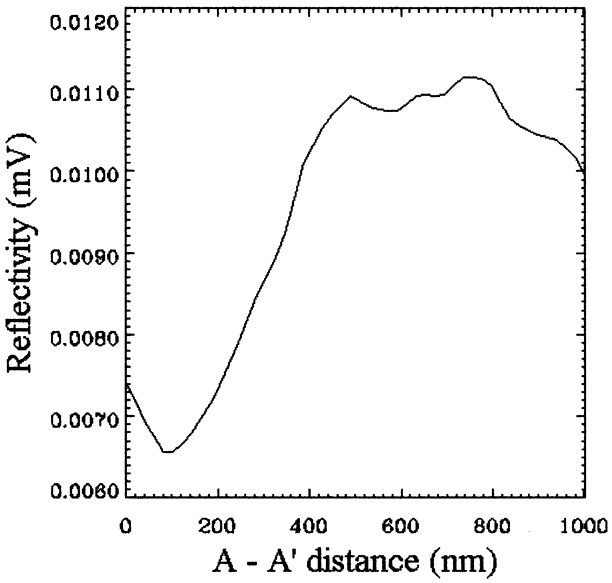

Fig. 4. Profile taken along the A–A′ line on the reflectivity image taken with $\lambda = 3.5$ μm in Fig. 3(c).

images even in the absence of one-to-one correspondence between the two images. This is why it is important to measure the same SNOM image by changing the photon energy: in fact, the same topography will induce the same shadow effects in SNOM images taken with different photon energy. The two SNOM images presented in Figs 3(a) and (e) indicate that this is not the case, as these two images are different from that in Fig. 3(c). In the presence of topographical shadow effects the three SNOM images in Figs 3(a), (c) and (e) would be the same. The fact that they are different proves that this is a real optical effect.

Furthermore, we work in ambient conditions so that we cannot avoid water absorption at the surface of the sample and also on the optical fibre, as is true for all the SNOM microscopes working in air. Here again it is important to perform SNOM spectroscopy to check a possible water contribution. However, there is nothing special for water absorption between 3.2, 3.5 and 3.7 μm so that we would expect the same contribution from water in the three SNOM images taken with the above wavelengths: the fact that the two SNOM images presented in Figs 3(a), (e) are different from the one represented in Fig. 3(c) rules out this possibility.

Note that dark spots in the on-absorption SNOM Fig. 3(c) do not correspond to the highest elevations of the topographic Fig. 3(d), but rather to the valleys. i.e. to the grain boundaries between the diamond crystallites. This is reasonable in light of the literature results on hydrogen in CVD diamond films.

It is interesting to analyse the lateral resolution of the topographic and spectroscopic-SNOM images. For the topographic images, line scans yield resolution estimates between 50 and 80 nm, demonstrating the high quality of the fibre tips. By contrast, similar line scans for the spectroscopic SNOM images (see the slope in Fig. 4) demonstrate a lateral resolution of 200 nm, which is well below the classical microscopy limit ($\lambda/2$). A value better than $\lambda/15$ can, then, be derived at 3.5 μm.

Why are the off-absorption SNOM images in Figs 3(a) and (e) so dramatically featureless with respect to the on-absorption Fig. 3(c)? The answer is that diamond is quite transparent to the infrared light in this spectral range. The near-field waves decay exponentially independent of absorption, but strong absorption enhances this effect, producing excellent SNOM images. In a sense, therefore, an on-absorption image such as Fig. 3(c) is a case of enhanced SNOM regime, yielding high chemical contrast.

This successful test of spectroscopic SNOM is interesting on its own, as it lends credibility to the suspicion that hydrogen is in fact present in many systems that are nominally hydrogen-free. But its impact is much more general: spectroscopic SNOM can be applied, for example, in biology and polymer science, as well as to lateral chemical fluctuations of buried semiconductor interfaces (Margaritondo *et al.*, 1993). In the latter case, FEL-based SNOM techniques can reveal not only lateral chemical fluctuations but also the corresponding changes in interface energy barriers, functioning as a uniquely complete probe on a microscopic scale.

Acknowledgements

We would like to thank the entire staff of the Vanderbilt FEL centre for their essential help. Work supported by the Italian National Research Council (CNR), by the Ecole Polytechnique Fédérale de Lausanne and by the Fonds National Suisse de la Recherche Scientifique. The Vanderbilt FEL centre is a national facility supported by the US Office of Naval Research.

References

Almeida, J., dell'Orto, T., Coluzza, C., Margantondo, G., Bergossi, O., Spajer, M. & Courjon, D. (1996) Novel spectromicroscopy: Pt-GaP studies by spatially resolved internal photoemission with near-field. *Appl. Phys. Lett.* **69**, 2361–2363.

Angus, J.C., Will, H.A. & Stanko, W.S. (1968) Growth of diamond seed crystals by vapor deposition. *J. Appl. Phys.* **39**, 2915–2922.

Betzig, E. & Trautman, J.K. (1992) Near-field optics: microscopy,

spectroscopy, and surface modification beyond the diffraction limit. *Science*, **257**, 189–195.

Betzig, E., Finn, P.L. & Wiener, J.S. (1994) Combined shear force and near-field scanning optical microscopy. *Appl. Phys. Lett.*, **60**, 2484–2486.

Coluzza, C., Tuncel, E., Staehli, J.L., Baudat, P.A., *et al.* (1992) Interface measurements of heterojunction band lineups with the Vanderbilt free-electron laser. *Phys. Rev. B*, **46**, 12834–12836.

Cricenti, A., Generosi, R., Perfetti, P., Gilligan, J.M., Tolk, N.H., Coluzza, C. & Margaritondo, G. (1998a) Free-electron laser near-field nanospectroscopy. *Appl. Phys. Lett.*, **73**, 151–153.

Cricenti, A., Generosi, R., Barchesi, C., Luce, M. & Rinaldi, M. (1998b) A multipurpose scanning near-field optical microscope: reflectivity and photocurrent on semiconductor and biological samples. *Rev. Sci. Instrum.* **69**, 3240–3244.

Heinzelmann, H. & Pohl, D.W. (1994) Scanning near-field optical microscopy. *Appl. Phys. A*, **59**, 89–101.

Margaritondo, G., Gozzo, F. & Coluzza, C. (1993) Band bending at semiconductor interfaces and its effect on photoemission line shapes. *Phys. Rev. B*, **47**, 9907–9909.

Mossadegh, R., Sanghera, J.S., Schaafsma, D.T., Cole, B.J., Nguyen, V.Q., Miklos, R.E. & Aggarwal, I.D. (1998) Fabrication of single mode chalcogenide optical fiber. *J. Lightwave Technol.* **16**, 214–217.

Pohl, D.W. & Courjon, D., eds (1992) *Near Field Optics*, **Vol. 262**. NATO ASI Series. Kluwer Academic Press, Dordrecht.

Tuncel, E., Staehli, J.L., Coluzza, C., Margantondo, G., McKinley, J.T. *et al.* (1993) Free-electron laser studies of direct and indirect two-photon absorption in germanium. *Phys. Rev. Lett*. **70**, 4146–4149.